Quaternary Science Reviews 78 (2013) 155–168

Contents lists available at ScienceDirect

Quaternary Science Reviews

journal homepage: www.elsevier.com/locate/quascirev

A Stalagmite record of Holocene Indonesian–Australian summer monsoon variability from the Australian tropics

Rhawn F. Denniston [a,*], Karl-Heinz Wyrwoll [b], Victor J. Polyak [c], Josephine R. Brown [d], Yemane Asmerom [c], Alan D. Wanamaker Jr. [e], Zachary LaPointe [c], Rebecca Ellerbroek [a], Michael Barthelmes [a], Daniel Cleary [a], John Cugley [f], David Woods [g], William F. Humphreys [b,h,i]

[a] *Department of Geology, Cornell College, Mount Vernon, IA, USA*
[b] *University of Western Australia, Perth, Western Australia, Australia*
[c] *Department of Earth and Planetary Sciences, University of New Mexico, Albuquerque, NM, USA*
[d] *Centre for Australian Weather and Climate Research, Melbourne, Australia*
[e] *Department of Geological and Atmospheric Sciences, Iowa State University, Ames, IA, USA*
[f] *Kimberley Toad Busters, Kununurra, Western Australia, Australia*
[g] *Department of Environment and Conservation, Broome, Western Australia, Australia*
[h] *Western Australian Museum, Welshpool DC, Western Australia, Australia*
[i] *University of Adelaide, Adelaide, South Australia, Australia*

ARTICLE INFO

Article history:
Received 22 April 2013
Received in revised form
7 August 2013
Accepted 8 August 2013
Available online 6 September 2013

Keywords:
Stalagmite
Oxygen isotope
Indonesian–Australian summer monsoon
El Nino-Southern Oscillation
Intertropical convergence zone
Holocene

ABSTRACT

Oxygen isotopic data from a suite of calcite and aragonite stalagmites from cave KNI-51, located in the eastern Kimberley region of tropical Western Australia, represent the first absolute-dated, high-resolution speleothem record of the Holocene Indonesian–Australian summer monsoon (IASM) from the Australian tropics. Stalagmite oxygen isotopic values track monsoon intensity via amount effects in precipitation and reveal a dynamic Holocene IASM which strengthened in the early Holocene, decreased in strength by 4 ka, with a further decrease from ∼2 to 1 ka, before strengthening again at 1 ka to years to levels similar to those between 4 and 2 ka. The relationships between the KNI-51 IASM reconstruction and those from published speleothem time series from Flores and Borneo, in combination with other data sets, appear largely inconsistent with changes in the position and/or organization of the Intertropical Convergence Zone (ITCZ). Instead, we argue that the El Niño/Southern Oscillation (ENSO) may have played a dominant role in driving IASM variability since at least the middle Holocene. Given the muted modern monsoon rainfall responses to most El Niño events in the Kimberley, an impact of ENSO on regional monsoon precipitation over northwestern Australia would suggest non-stationarity in the long-term relationship between ENSO forcing and IASM rainfall, possibly due to changes in the mean state of the tropical Pacific over the Holocene.

1. Introduction

The modern climate of the Australian tropics is dominated by the IASM, part of an extensive monsoon system ranging across the Maritime Continent and the Indo-Pacific Warm Pool (IPWP) and extending southwards into northern Australia (Fig. 1). The IASM serves as a major tropical heat source that plays a significant role in the planetary scale circulation and is strongly linked to its East Asian Summer Monsoon (EASM) counterpart (McBride, 1987; Neale and Slingo, 2003; Chang et al., 2004). Marine and continental paleoclimate studies have reconstructed the IASM at millennial scales during the Last Glacial, and produced a largely consistent pattern of IASM variability in which the IASM trough, which is tied to positioning of the ITCZ, was displaced latitudinally due to changes in North Atlantic climate and meridional ocean circulation (Partin et al., 2007; Griffiths et al., 2009; Lewis et al., 2010; Muller et al., 2012; Denniston et al., 2013) (Table 1).

For the Holocene, a more complex regional picture of monsoon events over the wider IASM and EASM regions has begun to emerge in which: (i) stalagmites from Dongge Cave, China (25°N, 108°E)

* Corresponding author.
E-mail address: rdenniston@cornellcollege.edu (R.F. Denniston).

0277-3791/$ – see front matter
http://dx.doi.org/10.1016/j.quascirev.2013.08.004

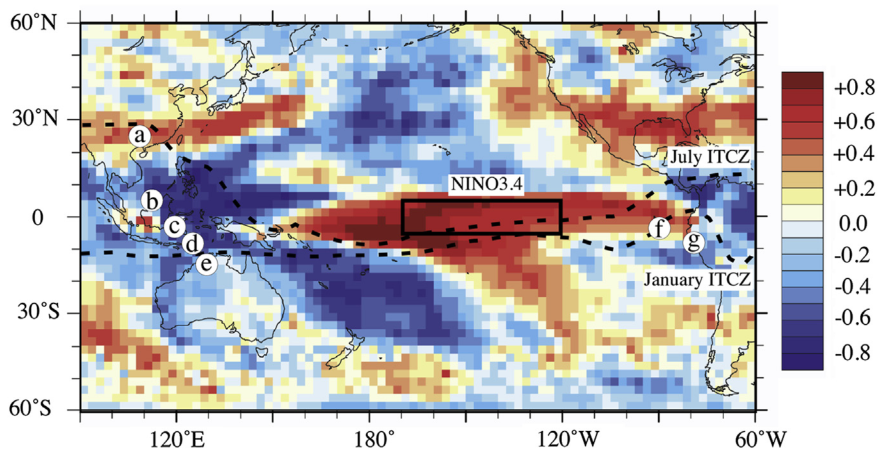

Fig. 1. Map of the Pacific Basin showing correlations between regional rainfall anomalies and NINO3.4 (box) SST for the years 1979–2008 based on the GPCP database. Stalagmite records of Holocene monsoon variability cited in text are: a. Dongge Cave (Wang et al., 2005); b. Gunung Buda, Borneo (Partin et al., 2007); c. Sulawasi (Tierney et al., 2012); d. Liang Luar, Flores (Griffiths et al., 2009); e. KNI-51 (this study); f. El Junco, Galapagos (Conroy et al., 2008); g. Laguna Pallcacocha, Ecuador (Moy et al., 2002).

record decreases in EASM strength during the Holocene in close agreement with reductions in precession-driven summer insolation in the Northern Hemisphere (Wang et al., 2005); (ii) stalagmites from Gunung Buda, Borneo (5°N, 114°E) reveal IASM strength that tracked differences in fall and spring insolation, with peak rainfall during the middle Holocene (Partin et al., 2007); (iii) stalagmites from Liang Luar, Flores (8°S, 120°E) record a middle Holocene characterized by a period of reduced rainfall, opposite in sign to the Borneo record, and attributed to regional SST variations associated with the Indian Ocean Dipole (IOD; Griffiths et al., 2010);

Table 1
U/Th Isotopic Ratios and ^{230}Th Ages of KNI-51 Stalagmites.

Sample	Mineral	Distance to base (mm)	^{238}U (ng/g)	^{232}Th (pg/g)	δ^{234}U[a] (corr'd)	Error[b]	^{230}Th/^{238}U (activity)	Error	^{230}Th/^{232}Th (ppm)	Error	Uncorrected Age (yr)	Error (yr)	Corrected[c] Age (yr)	Age[d] (yr BP)	Error (yr)
0	Calcite	192	422	15,569	409.7	2.0	0.014	0.00034	6.4	0.2	1109	27	345	285	764
0	Calcite	181	84	3988	450.3	5.0	0.065	0.00241	22.7	0.9	5006	191	4054	3994	972
0	Calcite	173	183	3261	444.2	2.0	0.061	0.00073	56.7	0.9	4752	58	4392	4332	365
0	Calcite	156	452	5793	424.3	1.3	0.067	0.00055	86.7	1.1	5297	45	5034	4974	266
0	Calcite	148	106	2196	460.0	2.4	0.070	0.00133	55.5	1.5	5360	105	4945	4885	428
0	Calcite	141	122	1113	446.0	2.6	0.070	0.00139	126.2	6.1	5426	111	5242	5182	215
0	Calcite	108	100	2518	474.8	1.9	0.079	0.00110	51.4	1.5	6003	86	5502	5442	508
0	Calcite	106	112	1207	480.4	1.8	0.079	0.00110	121.5	3.9	6021	86	5809	5749	229
0	Calcite	97	72	1427	441.5	2.2	0.080	0.00180	66.4	2.4	6250	144	5847	5787	427
0	Calcite	77	136	579	506.0	2.0	0.108	0.00076	418.3	15.4	8130	60	8048	7988	102
0	Calcite	64	82	2020	445.7	2.9	0.098	0.00220	65.5	2.5	7664	179	7167	7107	528
0	Calcite	54	84	429	457.5	2.4	0.114	0.00168	366.0	32.4	8889	138	8787	8727	172
0	Calcite	44	89	2222	458.3	2.3	0.111	0.00149	73.3	1.7	8663	122	8164	8104	514
0	Calcite	36	136	579	506.0	2.0	0.108	0.00076	418.3	15.4	8130	60	8048	7988	102
3	Aragonite	687	4494	17,629	994.6	2.0	0.056	0.00008	234.1	0.7	3095	5	3037	2977	29
3	Aragonite	245	6994	3166	938.6	1.9	0.056	0.00009	2049.4	41.2	3219	6	3212	3152	7
3	Aragonite	5	5411	3375	969.7	2.0	0.069	0.00010	1830.4	41.3	3914	7	3904	3844	8
4	Calcite	475	91	2717	461.6	1.6	0.106	0.00086	58.3	0.6	8233	70	7634	7574	602
4	Calcite	315	99	1041	453.5	2.3	0.102	0.00090	160.2	4.1	7934	74	7724	7664	222
4	Calcite	307	119	1589	492.9	1.7	0.106	0.00090	131.5	2.4	8079	72	7819	7759	269
4	Calcite	240	135	2104	506.4	1.3	0.113	0.00083	119.7	1.8	8566	66	8264	8204	309
4	Calcite	216	154	3979	488.5	1.4	0.115	0.00075	73.6	0.7	8821	60	8315	8255	509
7	Aragonite	1021	4434	1246	1345.0	1.4	0.049	0.00019	2851.9	65.0	2288	9	2285	2225	10
7	Aragonite	527	4376	1355	1337.3	1.6	0.059	0.00041	3139.8	134.6	2792	20	2789	2729	20
7	Aragonite	57	11,822	21,578	1302.6	1.5	0.066	0.00027	593.9	2.5	3167	13	3143	3083	27
10	Aragonite	617	2238	54,450	1654.6	1.8	0.017	0.00013	11.7	0.1	710	5	443	383	267
10	Aragonite	414	2651	27,445	1658.1	1.8	0.021	0.00012	33.9	0.2	877	5	763	703	113
10	Aragonite	357	2520	33,068	1616.1	2.7	0.028	0.00014	35.6	0.2	1187	6	1041	981	146
10	Aragonite	134	2213	27,637	1569.2	1.5	0.031	0.00022	40.8	0.3	1319	9	1177	1117	142
10	Aragonite	12	2488	122,539	1630.5	8.3	0.043	0.00017	14.3	0.1	1782	9	1236	1176	546
11	Aragonite	41	10,238	1488	1338.4	1.1	0.00003	0.00001	3.8	1.5	2	1	0	−60	2
11	Aragonite	30	6049	643	1380.3	1.0	0.001	0.00002	215.5	11.8	64	1	62	2	2
11	Aragonite	21	6382	579	1358.8	1.9	0.002	0.00003	446.8	32.1	114	1	113	53	2
11	Aragonite	9	4686	4432	1359.9	1.7	0.005	0.00004	82.4	1.0	219	2	207	147	12
11	Aragonite	4	5321	6216	1354.6	1.9	0.005	0.00005	72.2	0.8	237	2	223	163	15
A1	Aragonite	530	3688	26,213	1012.8	2.0	0.066	0.00014	153.8	0.8	3662	9	3559	3499	103
A1	Aragonite	304	8154	2875	900.8	1.9	0.062	0.00008	2894.1	93.4	3619	6	3613	3553	8
A1	Aragonite	24	4646	649	1098.0	2.1	0.070	0.00012	8282.9	801.9	3721	7	3719	3659	8
A2-side 1	Aragonite	17	12,576	10,201	943.8	2.0	0.083	0.00012	1689.1	7.0	4780	9	4768	4708	15
A2-side 1	Aragonite	2	7032	8832	995.2	2.0	0.086	0.00013	1132.1	11.0	4834	9	4816	4756	20